



Available Online through
www.ijptonline.com

METHODS FOR AUTOMATIC PROCESSING AND ANALYSIS OF ORTHOTROPIC BIOLOGICAL STRUCTURES BY MICROSCOPY AND COMPUTED TOMOGRAPHY

Shigapova A. Faina*, Baltina V. Tat'yana, Konoplev G. Yuriy, Sachenkov A. Oskar

Kazan Federal University, 18, Kremlyovskaya St., Kazan, (420008) Russia.

Email: 4works@bk.ru

Received on 13-07-2016

Accepted on 10-08-2016

Abstract:

Image acquisition and analysis is a key moment in the biological research and diagnostics. In practice, the evidence-based medicine and biology have to deal with large arrays of image data. Automating these data processing is a relevant task. This paper presents a software package that performs automated processing of biological objects with a pronounced orthotropy. As well as the results of such data processing for two-dimensional setting - analysis of the structure of the skin and muscles, as well as for three-dimensional analysis - processing of bone tissue tomograms. To analyze the properties of orthotropy, we used a mathematical apparatus designed on the basis of anisotropic tensor, the use of which ensures estimation of the averaged direction of the periodic structure in the plane or space, their frequency and the filling density. The versatility and availability of automated mode ensures significant acceleration of data processing and improves the quality of the results.

Keywords: biomechanics, orthotropic biological structures, process automation, image analysis, anisotropic tensor.

Introduction

Image acquisition and analysis is a key moment in the biological research and diagnostics. There are two types of hardware and computer systems for medical imaging.

The first type includes, primarily, a digital X-ray diagnostic apparatuses with digital terminal. They digitize an image and transfer it to a workstation for further analysis. X-ray films are one of the leading methods of diagnosing patients. This type also includes ultrasound hardware and computer systems. The resulting images here, also called sonograms, are less clear, however, more affordable diagnostic method due to the cheapness of their acquisition process.

The second type is based on the reconstruction of three-dimensional models of organs based on the original digital images. It includes a computed tomography (CT) and magnetic resonance imaging (MRI). The first provides layered images of human internal organs when moving an X-ray tube around the patient's body. The scanning technique allows

making instantly a large number of slices at 1-5 mm interval. MRI is based on the study of nuclear magnetic resonance of human protons placed in a strong magnetic field. Here the examples of practical data processing:

1. Subtraction. Digital subtraction angiography (DSA). First, an X-ray of the studied area is performed, then – its negative inversion and radiopaque image of blood vessels – angiography. Then the first image is subtracted from the second image to obtain the image of vessels (Fig. 1).

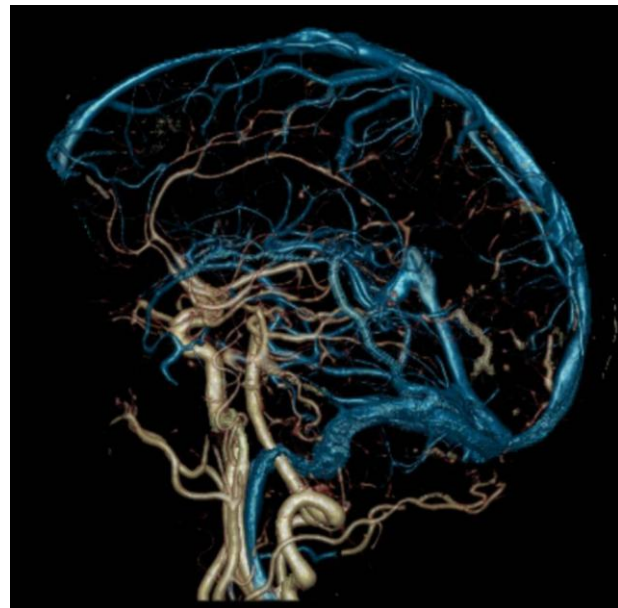


Fig. 1. Brain angiogram.

2. Two-photon X-ray computed osteodensitometry. The computer evaluates the difference in X-ray absorption capacity and quantifies the skeletal bone mineral density. This allows identifying risk area of fracture, as well as diagnosing osteoporosis at an early stage (Fig. 2).

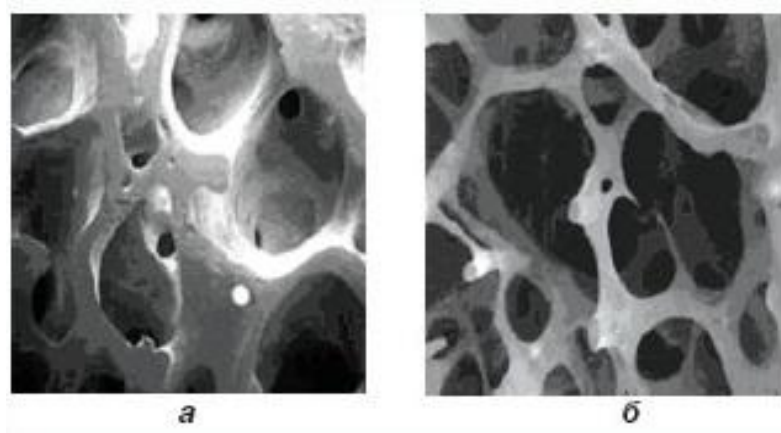


Fig. 2 Normal state and osteoporosis.

Biometric security systems (intelligent recognition methods and the use of neural networks). Biometric technologies are based on biometrics - the measurement of the unique characteristics of the individual person. These can be both unique congenital features (DNA, fingerprints, iris), and characteristics, acquired with time or changing with age or

Biometrics operates with several proven methods. The most widespread is a method of flexible graphs. Recognition is performed by comparing the facial contours. In this method, a face is represented as a graph, which nodes are located at key points of the face. Each face is marked with the distances between its nodes. In each of these points, the Gabor expansion coefficients are calculated for five different frequencies and eight orientations.

All solutions described have software implementation, but the data processing is always ultimately accompanied by an operator, which chooses the desired solution from the selected palette and applies it to the image. Process automation in this case remains at the level of implementation of the selected mathematical apparatus, and the routine data processing and acquisition is performed by the operator. When processing more data, both labor expended and time costs remain at the same level, however an operator error factor increases.

Methods

Automation of the graphic image analysis process ensures optimization of research, reduces overheads for routine data processing, as well as improves the quality of information - the accuracy of the results, which is an urgent task in identifying statistical laws. The vast majority of mechanics' problems is associated with finding the stress-strain state. For isotropic materials, elastic tensor degenerates into a Young's modulus and Poisson's ratio. However, anisotropic materials require to build a fourth-rank tensor.

The most successful modern way of describing the structure of porous and composite materials is a symmetric positive definite second-rank tensor, called the structure tensor and denoted as \tilde{H} [1, 2]. It is uniquely determined by its projections on three mutually perpendicular planes. The structure tensor allows describing the tissue anisotropy, and its principal values allow characterizing the distribution of the material along the main directions. The structure tensor allows describing the structural features of any human tissue.

A quantitative description of the tissue structure can be done by stereology methods [3]. All measurements are performed on the image. The targeted stereometric value – the average distance between the pores L – allows us to describe the anisotropy degree of the material. According to E. Underwood, the average distance between the pores is an average distance between the "environment-pore" boundaries, measured along a certain direction" [3-5]. To determine L in the θ direction, a grid consisting of parallel test lines is superimposed on a sample. The measurements are repeated in different θ directions. $\theta_1 = 0^\circ, \theta_2 = 120^\circ, \theta_3 = 240^\circ$ Is commonly selected (Fig. 3).

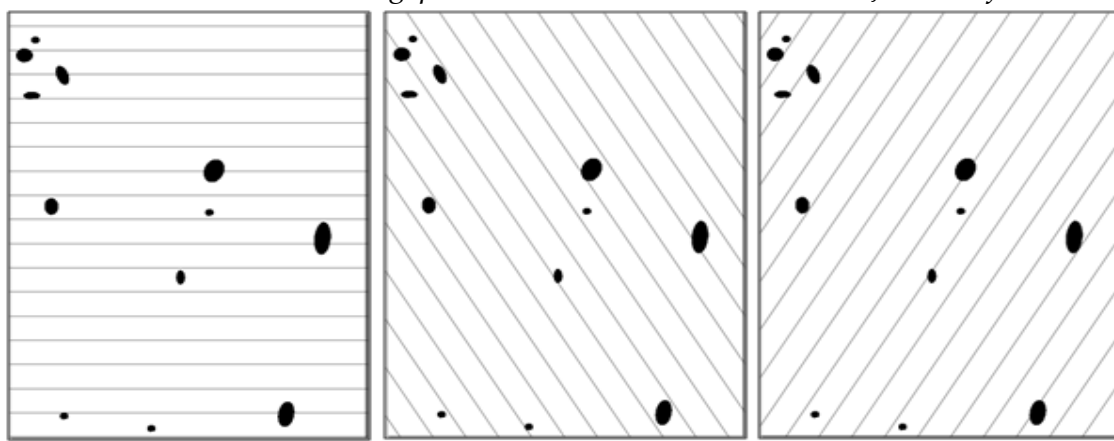


Fig. 3. Example of using the test grid for determining the average distance between the pores.

The average distance between the pores is commonly [6] calculated by the formula:

$$L_b(\theta) = 2 \frac{\sum l}{I(\theta)} A_{Ab}, \quad (1)$$

where $\sum l$ - the total length of all lines in the grid, $I(\theta)$ - the number of intersections of lines with the “environment-pore” boundaries, A_{Ab} - the relative area of the substance on the slice.

If we perform a set of measurements in different directions, we can obtain a sinusoidal distribution $L_b(\theta)$ [4-6]. The average distance between the pores as a function of direction $L_b(\theta)$ can be described by the ellipse equation:

$$\left(\frac{1}{L_b(\theta)}\right)^2 = \frac{m_{\alpha\alpha} + m_{\beta\beta}}{2} + \frac{m_{\alpha\alpha} - m_{\beta\beta}}{2} \cos 2\theta + m_{\alpha\beta} \sin 2\theta, \quad (2)$$

where indices α and β denote the axes e_α and e_β , respectively, in the coordinate system imposed on the plane (Fig. 4).

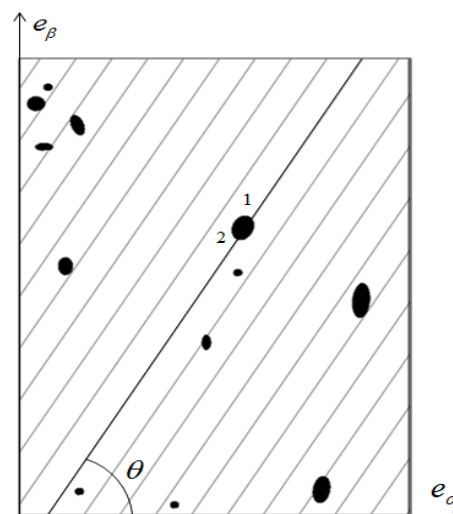


Fig. 4. Determining the average distance between the pores.

for the test line selected on the image in the system of coordinates ($e_\alpha - e_\beta$); points 1 and 2 - the intersection points of the selected line in the grid with an “environment-pore” boundary

In [4-6], it was shown that in the three-dimensional model the average distance between the pores $L_b(\theta)$ can be represented in the form of an ellipsoid:

$$\left(\frac{1}{L_b(\theta)}\right)^2 = \bar{n} \cdot \tilde{M} \cdot \bar{n}, \quad (3)$$

where \bar{n} – a unit vector in the direction of the test line, referred to as

$$\bar{n} = \cos \theta \bar{e}_\alpha + \sin \theta \bar{e}_\beta, \quad (4)$$

therefore, we can introduce an equivalent symmetric, second-rank positive definite tensor: anisotropic tensor \tilde{M} .

According to the theorem of the opposite tensor factor, $m_{\alpha\alpha}$, $m_{\beta\beta}$, $m_{\alpha\beta}$ are the components of the anisotropic tensor \tilde{M} , which in matrix representation has the form as follows

$$\tilde{M} = \begin{bmatrix} m_{11} & m_{12} & m_{13} \\ m_{21} & m_{22} & m_{23} \\ m_{31} & m_{32} & m_{33} \end{bmatrix} \quad (5)$$

If we denote the left-hand side of equation (2) as a certain function $f(\theta)$ and introduce the notations:

$$f_1 = f(\theta_l), \quad \psi_l = 2\theta_l, \quad l = 1, 2, 3, \quad (6)$$

where f_i – the values of the introduced function for the respective directions

θ_i , then the anisotropic tensor components $m_{\alpha\alpha}$, $m_{\beta\beta}$, $m_{\alpha\beta}$ can be determined as follows:

$$\begin{aligned} m_{\alpha\alpha} &= \frac{f_2(1-\cos\psi_1) - f_1(1-\cos\psi_2)}{\cos\psi_2 - \cos\psi_1} + \chi \cdot (\operatorname{ctg}\frac{\psi_1 + \psi_2}{2}) \cdot (1 - \cos\psi_1) - \sin\psi_1, \\ m_{\beta\beta} &= \frac{f_1(1+\cos\psi_2) - f_2(1+\cos\psi_1)}{\cos\psi_2 - \cos\psi_1} - \chi \cdot (\operatorname{ctg}\frac{\psi_1 + \psi_2}{2}) \cdot (1 + \cos\psi_1) + \sin\psi_1, \\ m_{\alpha\beta} &= \chi. \end{aligned} \quad (7)$$

Function χ introduced for easier presentation is written as

$$\chi = \frac{f_3 - k \cdot f_2 + f_1(k-1)}{\sin\psi_3 - k \cdot \sin\psi_2 + \sin\psi_1(k-1)}, \quad (8)$$

where k – coefficient, depending on the selected directions during stereological measurements:

Whereas, the following condition must be satisfied:

$$\frac{\sin(\psi_1 - \psi_2) + \sin(\psi_2 - \psi_3) + \sin(\psi_3 - \psi_1)}{2f_1f_2f_3} \neq 0 \quad . \quad (10)$$

Anisotropic tensors (11) for three mutually orthogonal faces of a three-dimensional sample can be used for building the tensor \tilde{M} .

$$\begin{pmatrix} m_{\alpha\alpha} & m_{\alpha\beta} \\ m_{\beta\alpha} & m_{\beta\beta} \end{pmatrix}_{1-2}, \begin{pmatrix} m_{\alpha\alpha} & m_{\alpha\beta} \\ m_{\beta\alpha} & m_{\beta\beta} \end{pmatrix}_{2-3}, \begin{pmatrix} m_{\alpha\alpha} & m_{\alpha\beta} \\ m_{\beta\alpha} & m_{\beta\beta} \end{pmatrix}_{1-3} \quad (11)$$

Components \tilde{M} are obtained with the use of the correction coefficients a_1, a_2, \dots, a_6 from ratios

$$\begin{aligned} m'_{11} &= a_1^2 (m_{\alpha\alpha})_{1-2} \\ m'_{22} &= a_2^2 (m_{\beta\beta})_{1-2} \\ m'_{33} &= a_4^2 (m_{\beta\beta})_{2-3} \\ m'_{12} &= a_1 a_2 (m_{\alpha\beta})_{1-2} \\ m'_{23} &= a_3 a_4 (m_{\alpha\beta})_{2-3} \\ m'_{13} &= a_5 a_6 (m_{\alpha\beta})_{1-3} \end{aligned} \quad . \quad (12)$$

Correction factors can be determined from (13).

$$\begin{aligned} a_1^2 (m_{\alpha\alpha})_{1-2} - a_5^2 (m_{\alpha\alpha})_{1-3} &= 0 \\ a_2^2 (m_{\beta\beta})_{1-2} - a_3^2 (m_{\alpha\alpha})_{2-3} &= 0 \\ a_4^2 (m_{\beta\beta})_{2-3} - a_6^2 (m_{\beta\beta})_{1-3} &= 0 \end{aligned} \quad . \quad (13)$$

We also need to introduce a constant C, which will reduce the computation error:

$$\begin{aligned} C^6 &= [(m_{\beta\beta} / m_{\alpha\alpha})_{1-2} (m_{\beta\beta} / m_{\alpha\alpha})_{2-3} (m_{\alpha\alpha} / m_{\beta\beta})_{3-1}] \\ a_1 / a_2 - C &= 0 \\ a_3 / a_4 - C &= 0 \\ a_6 / a_5 - C &= 0 \end{aligned} \quad . \quad (14)$$

The structure tensor \tilde{H} is algebraically related to the anisotropic tensor \tilde{M} . This relation is expressed by the formula

$$H = (M^{-1})^{\frac{1}{2}} \quad . \quad (15)$$

Obviously, the anisotropic ellipsoid projections on each face are ellipses (Fig. 5).

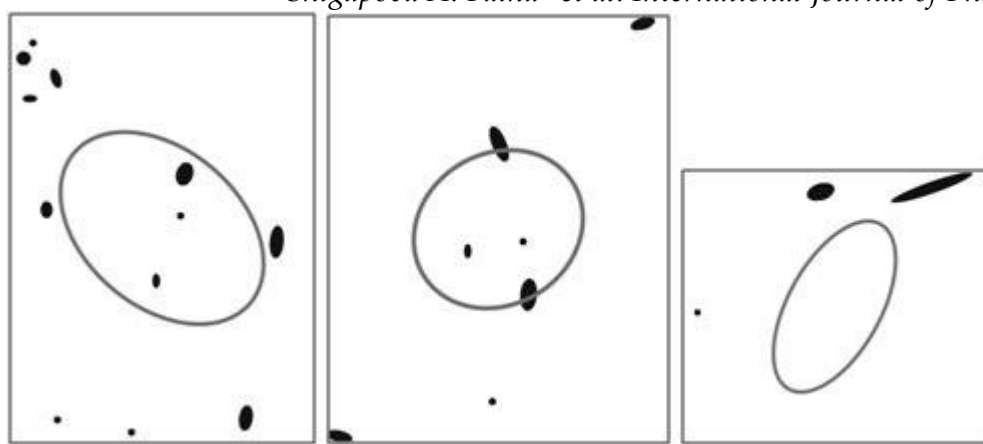
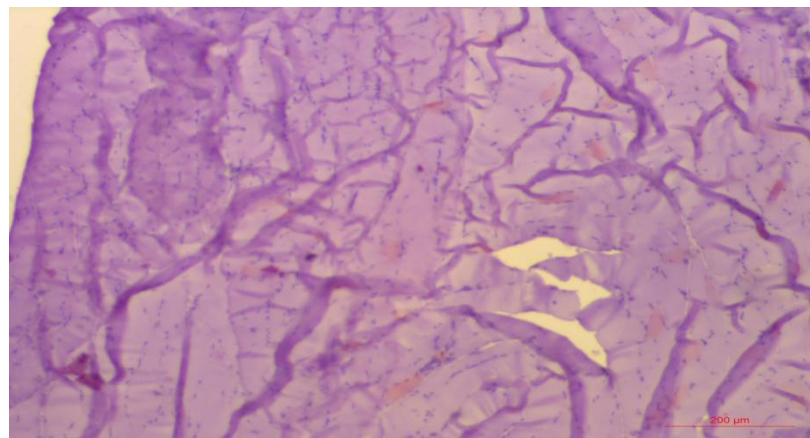


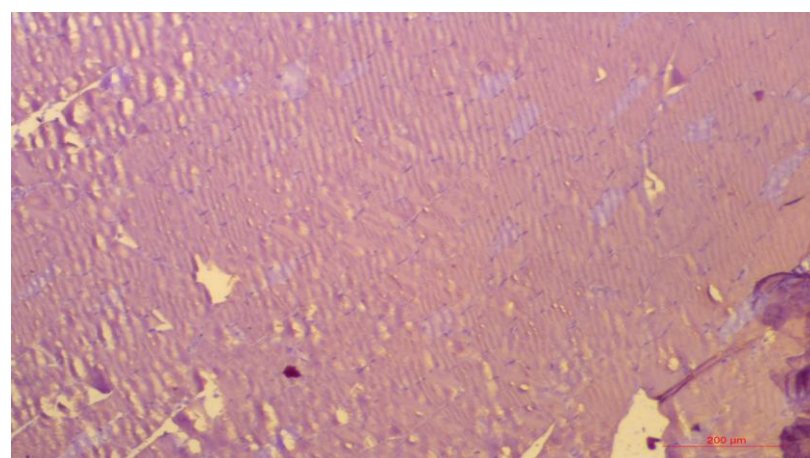
Fig. 5. the anisotropic ellipsoid projection on each face of the selected volume of a sample.

I. Results and Discussion

We shall consider the examples of biological image processing, and start with muscle tissue. It is known that human muscles are composed of muscle fibers, which in turn are divided into two fundamentally different types – fast and slow. The differences are both in the speed of involvement and in the source of energy used, and even in the fiber color. Slow (red) fibers, shown in Fig. 6a, are responsible for the long monotonous loads. Fast (white) fibers are required for short and high-intensity loads. They are shown in Fig. 6b.



a



b

Fig. 6. Muscle tissue: a – slow (red) fibers, b – fast (white) fiber.

The first stage involves differentiation of the areas in the image. Since all the test images have only two targeted types of material – fibers and the environment, it is convenient to use the black and white color palette - to binarize the images. The binarization threshold is usually determined by Kapoor entropy method [7].

During the following stage, we can start analyzing the image and determine the desired indicators, such as the size and number of muscle cells.

In our study, we also considered the analysis of images of the skin during scar healing. A scar develops through several stages [8]. During the first stage, the wound edges are connected with fragile granulation tissue. During the second stage, a newly-formed scar occurs. The granulation tissue begin to form collagen and elastin fibers. There remains an increased blood flow to the injury – the scar has rich pink color. The third stage is characterized by the disappearance of the vessels. The collagen fibers are arranged along the lines of greatest tension. The scar becomes lighter and denser. At the last stage, the final transformation of the scar occurs. Figure 7 shows an image of the scar at about stage 3 of formation.

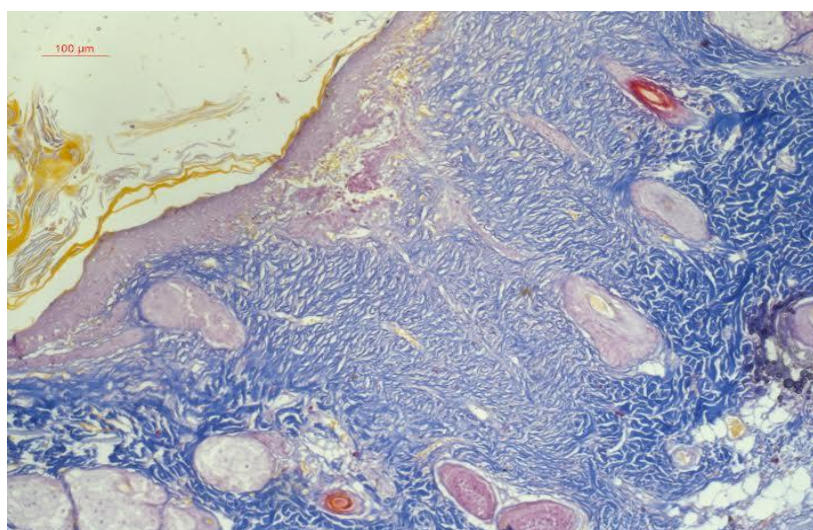


Fig. 7. A micrograph of a skin area around the scar edges.

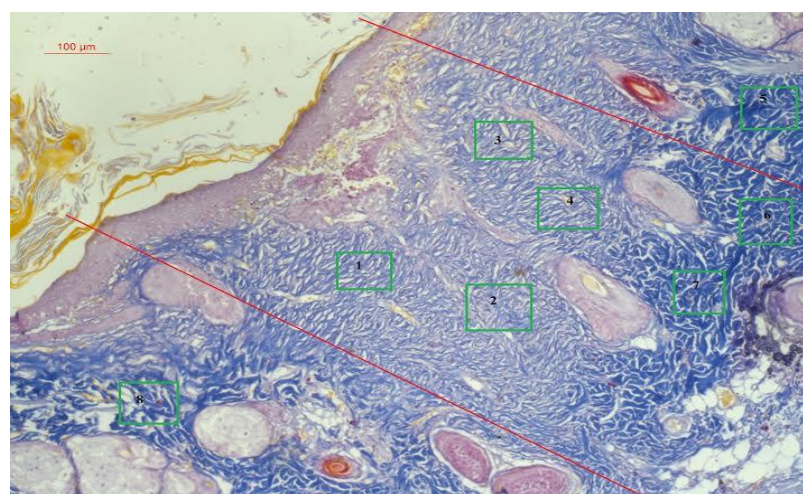


Fig. 8. Selection of subareas 1, 2, ..., 8 in the micrograph of a skin area.

Collagen fibers (blue area) are arranged along the edges of the wound. In this case, the structure tensor will numerically characterize the properties of collagen fibers. We shall distinguish several sub-areas (Fig. 8), build an anisotropy tensor for them, and show its main directions (Fig. 9). The angle between the perpendicular to the edge of the scar and the largest principal vector of anisotropy tensor is the smaller, the closer a sub-area is to the wound. The principal values at the same time allow estimating the severity of the characteristic structure of collagen.

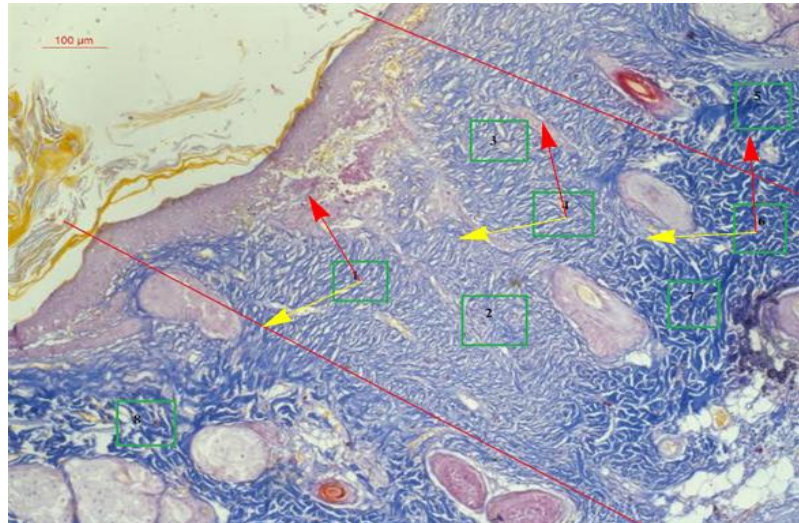


Fig. 9. The main directions of the anisotropy tensor in areas 1, 4 and 6.

The third task is to analyze the bone tissue. A characteristic feature in this case is that this causes processing of a large imaging array that includes a three-dimensional sample. It has been noted that the macroscopic parameters of bone tissue depend on its forming structure [9-11], and, based on external factors, the structure [11-13] can be reconstructed, and consequently the strength can be changed.

We have conducted the thigh bone scanning in the diaphysis and metaphysis; tests were performed with the use of micro/nanofocus X-ray inspection systems for computed tomography (CT) and 2D inspection Phoenix V|tome|X S240 in the laboratory of X-ray computed tomography of the Institute of Geology and Petroleum Technology of Kazan (Volga region) Federal University. Scanning resolution was 1-3 μm per voxel.

In the obtained scanning data, the cubic samples are identified – bone sub-areas with each face of less than one millimeter in size. Further, these samples are photographed in three orthogonal directions with a small pitch, so that about 80 images are obtained in each direction. Then, only these images are processed.

Conclusion

To handle large data arrays, an S-1 program module has been created, which ensured significant acceleration of the image processing and execution of mathematical operations.

This study was tested in the framework of the project of the study of hypogravity impact on the bone tissue structure.

We have formulated the task of determining the porosity and construction of the structure tensor of the bone tissue based on data of computed tomography. Figure 10 shows an example of micro-CT image in one of three orthogonal scanning directions.

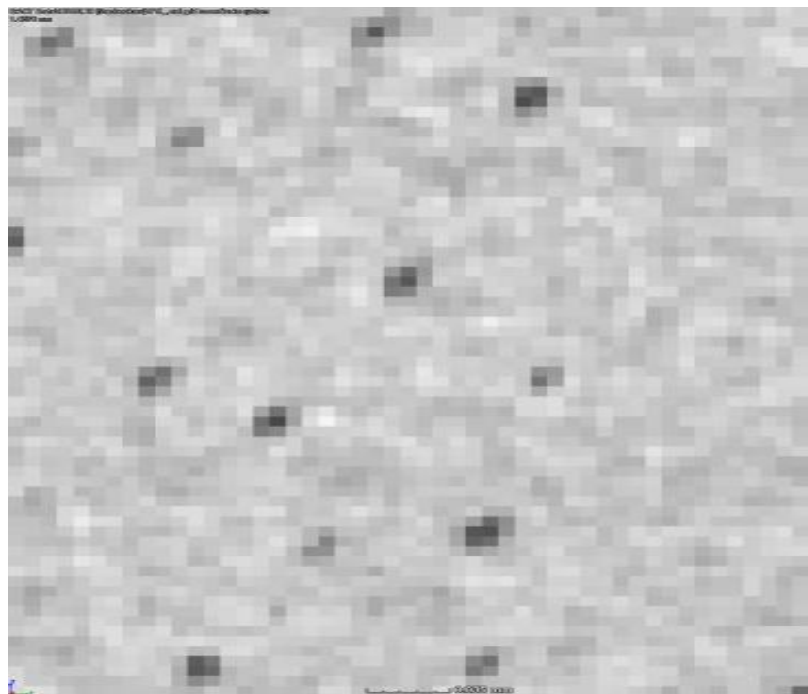


Fig. 10. Micro-CT image along one of three mutually orthogonal scanning directions of a bone cubic area.

All computations related to the calculation of the grid lengths, the number of intersections with their pores, the multiplication of inverse matrices and other mathematical operations are performed automatically with software package. In addition, we determined the porosity of bone tissue sample in the entire volume. For this purpose, we determined the relative area of the pores in each image and further integrated this value across the entire stack of images. We defined 8 samples in the diaphysis section. Thus, we had to process nearly two thousands of images. This took only about 10 minutes.

Summary

The developed module ensures automated processing of graphic images. This reduces the processing time of one image by 1-2 thousand times. Operator error rate decreases also. The versatility of the software allows working with images, regardless of the nature of their origin. The versatility of S1 program complex allows using it also for other types of related tasks. The module can be used for biological and medical research: the differentiation of the cell structures of the extracellular substance or other structures by various selection criteria (color, size, perimeter, center of gravity, etc.); angiograms analysis; osteodensitometry analysis (diagnosis of osteoporosis); and assessment of the bone bearing capacity, etc.

Acknowledgements

The work is performed according to the Russian Government Program of Competitive Growth of Kazan Federal University and the work was partially supported by the Russian Foundation for Basic Research within scientific projects No. 16-04-00772.

References.

1. Cowin S.C. An evolution Wolff's law for trabecular architecture // *J. Biomech. Engng.* – 1992. – Vol. 114. – Pp. 129–136.
2. Cowin S.C. Wolff's law of trabecular architecture at remodeling equilibrium // *J. Biomech. Engng.* – 1986. – Vol. 108. – Pp. 83–88.
3. Kanatani K. Stereological determination of structural anisotropy // *Int. J. Eng. Sci.* – 1984. – Vol. 22. – 531 p.
4. Kichenko A.A., Tverier V.M., Nyashin Y.L., Simanovskaya E.Y., Elovikova A.N. Formation and elaboration of the classical theory of bone tissue structure description // *Russian Journal of Biomechanics*. 2008. Vol. 12, No. 1: 66-85.
5. Kichenko A.A., Tverier V.M., Nyashin Y.I., Osipenko M.A., Lokhov V.A. On application of the theory of trabecular bone tissue remodelling // *Russian Journal of Biomechanics*. 2012. Vol. 16, No. 4: 46-64.
6. Cowin S.C. *Bone mechanics handbook*. – Second edition. – New York: CRC Press, 2001. – 1136 p.
7. Kapoor A., Winn J. Located hidden random fields: learning discriminative parts for object detection // European Conference on Computer Vision: Proc. of the intern. conf. Graz, 2006. Vol. 3, Pp. 302-315.
8. Galliamova Iu.A., Kardashova Z.Z. Hypertrophic and keloid scars // *Attending doctor*. – 2009; 10: 20-30
9. Sachenkov O., Kharislamova L., Shamsutdinova N., Kirillova E. and Konoplev Yu. Evaluation of the bone tissue mechanical parameters after induced alimentary Cu-deficiency followed by supplementary injection of Cu nanoparticles in rats // *IOP Conference Series: Materials Science and Engineering* 98 (2015) 012015
doi:10.1088/1757-899X/98/1/012015
10. Shigapova F.A., Mustakimova R.F., Saleeva G.T. and Sachenkov O.A. Definition of the intense and deformable jaw state under the masseters hyper tone // *International Journal of Applied Engineering Research* Vol.10 №24 pp. 44711-44714
11. Wolff J. *Das Gesetz der Transformation der Knochen*. – Berlin: Hirshwald, 1892. – 416 p.

12. Cowin S.C. Fabric dependence of an anisotropic strength criterion // J. Mech. Materials. – 1986. – Vol. 5. – Pp.

251–260.

13. Cowin S.C. The relationship between the elasticity tensor and the fabric tensor // J. Mech. Materials. – 1985. – Vol.

4. – Pp. 137–147.

Corresponding Author:

Shigapova Faina Akhmetovna*,